


Cite this: *CrystEngComm*, 2021, 23, 5200

From $[B_6O_{13}]^{8-}$ to $[GaB_5O_{13}]^{8-}$ to $[Ga\{B_5O_9(OH)\}\{BO(OH)_2\}]^{2-}$: synthesis, structure and nonlinear optical properties of new metal borates†

Qi-Ming Qiu  and Guo-Yu Yang *

Three new metal borates, namely $K_{0.5}[B_6O_{10}] \cdot H_2O \cdot 1.5H_2O$ (1), $[GaB_5O_{10}] \cdot H_2O$ (2) and $NaCs[Ga\{B_5O_9(OH)\}\{BO(OH)_2\}]$ (3), have been synthesized under solvothermal conditions. Compound 1 features an intricate 3D framework composed of $[B_6O_{13}]^{8-}$ clusters, resulting in a 6-connected achiral *pcu* net. After introducing the organic gallium, one of the BO_4 groups of the $[B_6O_{13}]^{8-}$ cluster is substituted by a GaO_4 polyhedron to form the acentric $[GaB_5O_{13}]^{8-}$ cluster in 2. It also displays a high second-harmonic generation (SHG) response about approximately 2.6 times that of KH_2PO_4 (KDP), which is higher than those of aluminoborates (ABOs) containing the acentric $[AlB_5O_{13}]^{8-}$ cluster (0.3–2.1 times that of KDP). Dipole moment calculations have been carried out to confirm these results. In the process of trying to synthesize a new compound with a denser structure than 2, we have unexpectedly obtained 3 crystallized in the centrosymmetric (CS) space group, which shows a 1D structure constructed from the $[Ga\{B_5O_9(OH)\}\{BO(OH)_2\}]^{2-}$ cluster. This kind of low-dimensional structure is rare in gallo-borates (GBOs) as well as ABOs.

Received 1st June 2021,
Accepted 22nd June 2021

DOI: 10.1039/d1ce00719j

rsc.li/crystengcomm

Introduction

Borates are an important class of nonlinear optical (NLO) crystals mainly because they can easily crystallize in the non-centrosymmetric (NCS) space group and such structures are conducive to obtaining a large second-harmonic generation (SHG) response.^{1–13} Alumino-borates (ABOs) with diverse structures can be obtained by introducing Al atoms (belonging to the same group as B atoms) into borates. Compared with the B atom, Al has more abundant coordination modes, such as an AlO_4 tetrahedron, O_2AlO_3 triangular bipyramid, $OAlO_4$ tetragonal pyramid and AlO_6 octahedron.^{14–16} In 1973, Lehmann and Teske introduced Al atoms into a borate system for the first time, but did not perform detailed characterization.¹⁷ After that, Xu *et al.* reported several cases of ABOs, but due to the lack of high-quality crystals, the precise structure of the compound has not been determined.^{18–21} Lin *et al.* also successfully synthesized a series of PKU-*n* (*n* = 1, 2, 5, 6, 8) ABOs with an open framework by a boric acid flux synthesis method, and their structures were mostly determined by powder X-ray

diffraction.^{22–26} Since 2009, our group has been committed to the synthesis of ABOs with special configurations oriented by organic amines or transition metal complexes.^{8,27,28} We introduce Al atoms into the borate framework based on the following considerations: (1) expanding the structural dimension of borates. The borate synthesized by a hydro(solvo)thermal method often exhibits a low-dimensional structure, and the introduction of Al is an effective way to form a multi-dimensional borate; (2) a twisted structure can be formed between Al and O atoms, thus forming a metal polyhedral configuration with a chiral center. The synergistic combination between acentric oxoboron clusters and chiral polyhedra (such as AlO_4 , GeO_4 or GaO_4 tetrahedra) is beneficial for increasing the probability of products crystallized in the NCS space group; (3) enriching the fundamental building blocks (FBBs) of borate, laying the foundation for the synthesis of more borate with unique FBBs and excellent properties. According to the above ideas, we have synthesized a new inorganic–organic hybrid solid with NLO properties, namely $[Zn(dap)_2][AlB_5O_{10}]$ (*dap* = 1,3-diaminopropane) under solvothermal conditions based on the structural features of 3D open framework inorganic solids and 2D metal–organic coordination polymers for the first time.²⁹ In addition, we also use the “vacancy-oriented synthesis strategy” to construct multicomponent composite polyoxometalates containing new $\{B_9O_{18}(OH)_3\}$ and $\{B_{22}O_{42}\}$ clusters.³⁰ The existing borates can only form $\{B_9O_{13}(OH)_4\}$, $\{B_9O_{12}(OH)_6\}$, $\{B_9O_{19}\}$, $\{B_9O_{17}(OH)_2\}$ and $\{B_9O_{16}(OH)_3\}$ clusters in previous studies.

MOE Key Laboratory of Cluster Science, School of Chemistry and Chemical Engineering, Beijing Institute of Technology, Beijing 100081, China.

E-mail: ygy@bit.edu.cn; Fax: (+86)10 6891 8572

† Electronic supplementary information (ESI) available: IR, TGA, and UV-vis spectra and PXRD patterns. CCDC 1962950, 2077862 and 2077863 for compounds 1–3. For ESI and crystallographic data in CIF or other electronic format see DOI: 10.1039/d1ce00719j

The Ga atom, like Al, belongs to the same main group elements and also has several coordination modes (*i.e.*, a GaO_4 tetrahedron, an O_2GaO_3 triangular bipyramid, and a GaO_6 octahedron).^{31–33} In our previous work, we found that the NLO properties of dense structures are better.^{34,35} Compared with the Al atom, Ga has a larger atomic radius and more easily forms a dense structure, but the crystal structure of gallo-borates (GBOs) is more difficult to obtain than that of ABOs. In the synthesis of GBOs, we choose organic gallium compounds (*i.e.*, gallium acetylacetonate and gallium isopropoxide) instead of traditional inorganic gallium sources (*i.e.*, gallium oxide, gallium chloride and gallium nitrate) mainly based on the following points: (1) gallium acetylacetonate is easily dissolved in organic solvents (*i.e.*, ethylenediamine and 1,3-propanediamine); (2) gallium acetylacetonate may undergo a slowly hydrolysis reaction to obtain a GaO_4 tetrahedron with a chiral Ga center in the crystallization process; (3) the synergistic combination between chiral GaO_4 tetrahedra and acentric oxoboron clusters increase the likelihood of producing new acentric GBOs with a dense structure, offering us the opportunity for choosing the desired NLO materials from these candidates.

In this work, in the process of trying to synthesize a dense structure crystallized in the NCS space group, we have obtained the following three new metal borates, namely $\text{K}_{0.5}[\text{B}_6\text{O}_{10}]\cdot\text{H}_2\text{O}\cdot 1.5\text{H}_2\text{O}$ (1), $[\text{GaB}_5\text{O}_{10}]\cdot\text{H}_2\text{en}$ (2) and $\text{NaCs}[\text{Ga}\{\text{B}_5\text{O}_9(\text{OH})\}\{\text{BO}(\text{OH})_2\}]$ (3). Compound 1 shows an achiral 3D framework with $[\text{B}_6\text{O}_{13}]^{8-}$ clusters. After replacing BO_4 with chiral GaO_4 polyhedra, the compound is transformed into a NCS structure and new compound 2 presents good NLO activity (2.6 times that of KDP), which is better than previously reported ABOs (0.3–2.1 times that of KDP). Therefore, the introduction of a chiral polyhedron with a larger atomic radius may be an effective way to synthesize better NLO crystals. In order to obtain a denser structure, we try to fill the void of 2 with alkali (earth) metal ions and unexpectedly obtained a GBO with rare 1D chains (compound 3). The synthesis, structure and comparison of the above compounds will be discussed in detail.

Experimental section

Materials and measurements

All chemical reagents were commercially available and used without further purification. Commercial high purity KH_2PO_4 (KDP, 99.99%) and LiNbO_3 (99.99%) were purchased from Aladdin Co., Ltd., China. Fourier transform infrared (FTIR) spectra were recorded on a Nicolet iS10 FTIR spectrometer using a mixture of KBr and a sample wafer in the range of 4000–400 cm^{-1} . Powder X-ray diffraction studies were performed on a Bruker D8 Advance X-ray diffractometer. Optical diffuse reflectance spectra in the range of 200–800 nm were obtained *via* a Lambda-950 UV/vis-NIR spectrophotometer at room temperature. Thermogravimetric analyses (TGA) were conducted on a METTLER TGA/SDTA 851e thermal analyser under a constant flow of oxygen from

room temperature to 1000 °C at a heating rate of 10 °C min^{-1} . SHG measurements were performed with a Nd:YAG solid-state laser ($\lambda = 1064 \text{ nm}$) as the incident light source. Commercial high purity KDP and LiNbO_3 were used as the reference for SHG measurements. Ion-exchange reactions were performed by stirring the samples of as-synthesized compound 2 (50 mg) in 5 M LiCl, NaCl, KCl, MgCl_2 , CaCl_2 , and BaCl_2 solutions (10 mL) at room temperature for 12 h. The ion-exchanged products were recovered by filtration, washed with excess water, and dried in air. The Li, Na, K, Mg, Ca and Ba contents in the ion-exchanged products were determined by inductively coupled plasma optical emission spectroscopy (ICP-OES, Agilent 725 ICP-OES).

Synthesis of $\text{K}_{0.5}[\text{B}_6\text{O}_{10}]\cdot\text{H}_2\text{O}\cdot 1.5\text{H}_2\text{O}$ (1)

A mixture of H_3BO_3 (0.370 g, 6 mmol) and potassium *tert*-butoxide (0.112 g, 1 mmol) was added into pyridine (1.5 mL) and ethylenediamine (2 mL). After stirring for 15 min, the resulting mixture was sealed in a 25 mL Teflon-lined stainless steel autoclave, heated at 210 °C for 8 days, and then slowly cooled to room temperature. The colorless block crystals were obtained (yield 80% based on H_3BO_3). Elemental anal. (%) calcd. for $\text{B}_{12}\text{H}_{13}\text{KO}_{25}$: K 6.70, found: K 6.33.

Synthesis of $[\text{GaB}_5\text{O}_{10}]\cdot\text{H}_2\text{en}$ (2)

A mixture of compound 1 (0.104 g, 0.5 mmol) and gallium acetylacetonate (0.367 g, 1 mmol) was added into pyridine (1 mL) and ethylenediamine (1.5 mL). After stirring for 1 h, the resulting mixture was sealed in a 20 mL Teflon-lined stainless steel autoclave, heated at 210 °C for 8 days, and then slowly cooled to room temperature. The colorless block crystals were obtained (yield 50% based on 1).

Synthesis of $\text{NaCs}[\text{Ga}\{\text{B}_5\text{O}_9(\text{OH})\}\{\text{BO}(\text{OH})_2\}]$ (3)

A mixture of compound 2 (0.104 g, 0.3 mmol), sodium *tert*-butoxide (0.096 g, 1 mmol) and $\text{CsOH}\cdot\text{H}_2\text{O}$ (0.168 g, 1 mmol) was added into pyridine (1 mL) and ethylenediamine (1.5 mL). After stirring for 1 h, the resulting mixture was sealed in a 20 mL Teflon-lined stainless steel autoclave, heated at 210 °C for 8 days, and then slowly cooled to room temperature. The colorless block crystals were obtained (yield 48% based on 2).

Crystallographic data collection and refinement

The single crystal X-ray diffraction data for compounds 1–3 were collected at 296 K on a Bruker SMART CCD diffractometer equipped with graphite monochromatized $\text{Mo K}\alpha$ radiation ($\lambda = 0.71073 \text{ \AA}$). The structures were solved by direct methods and refined by the full-matrix least-squares method on F^2 using the SHELXL-2018 programs.³⁶ All non-hydrogen atoms were refined with anisotropic displacement parameters. The final structures were checked for possible missing symmetry with the PLATON program.³⁷ The detail

Table 1 Crystallographic data and structure refinements for compounds 1–3

Compound	1	2	3
Formula	B ₁₂ H ₁₃ KO ₂₅	C ₂ H ₁₀ B ₅ GaN ₂ O ₁₀	B ₆ H ₃ CsGaNaO ₁₃
<i>M</i> (mol ^{−1})	581.92	345.89	501.50
<i>T</i> (K)	296(2)	296(2)	296(2)
Crystal system	Cubic	Monoclinic	Triclinic
Space group	<i>Pa</i> 3̄ no. 205	<i>Pc</i> no. 7	<i>P</i> 1̄ no. 2
<i>a</i> (Å)	12.243(3)	6.686(5)	7.027(2)
<i>b</i> (Å)	12.243(3)	8.082(6)	8.039(2)
<i>c</i> (Å)	12.243(3)	10.485(8)	11.442(4)
α (°)	90	90	108.567(10)
β (°)	90	97.192(18)	93.633(11)
γ (°)	90	90	90.442(11)
<i>V</i> (Å ³)	1835.2(13)	562.2(7)	611.2(3)
<i>Z</i>	4	2	2
<i>F</i> (000)	1168	344	468
<i>D</i> _c (g cm ^{−3})	2.106	2.043	2.725
θ (°)	2.88–31.61	3.19–25.05	2.67–29.28
<i>R</i> _{int}	0.0498	0.0516	0.0557
Independent reflns	1006	1004	3278
Refined parameters	74	183	203
Flack parameters	—	0.03(4)	—
<i>GoF</i>	1.067	1.046	1.027
<i>R</i> ₁ ^a [<i>I</i> > 2σ(<i>I</i>)]	0.0502	0.0554	0.0439
w <i>R</i> ₂ ^b [<i>I</i> > 2σ(<i>I</i>)]	0.1350	0.1212	0.0898

$$^a R_1 = \sum ||F_o| - |F_c|| / \sum |F_o|. \quad ^b wR_2 = \{ \sum w[(F_o)^2 - (F_c)^2]^2 / \sum [w(F_o)^2] \}^{1/2}.$$

crystallographic data and selected bond distances for compounds 1–3 are summarized in Tables 1 and S1–S3,† respectively.

Results and discussion

Synthesis of the compounds

From a synthetic point of view, the title compounds 1–3 are related to the synthesis conditions. All the compounds were synthesized under solvothermal conditions (pyridine and ethylenediamine) at 210 °C for 8 days. In 1, the compound containing [B₆O₁₃]^{8−} clusters was synthesized with H₃BO₃ and potassium salt, resulting in a 3D framework with the centrosymmetric (CS) space group. Based on the idea of “the synergistic combination between oxoboron clusters and chiral polyhedra (such as GaO₄ tetrahedra) to obtain the product with the NCS space group and high-dimensional structure”, we tried to add organogallium to compound 1, hoping to obtain a 3D GBO which crystallizes in the NCS space group. Fortunately, one of the BO₄ groups of the [B₆O₁₃]^{8−} cluster was substituted by GaO₄ to form the acentric [GaB₅O₁₃]^{8−} cluster. So, compound 2 which crystallizes in the NCS space group is constructed from the [GaB₅O₁₃]^{8−} cluster and exhibits a 6-connected (6-c) 3D framework with (4¹²·6³) *pcu* topology, just similar to 1. Considering that the non-framework volume of 2 occupies 37.4% of the whole unit cell volume, a variety of alkali and alkaline earth metals with different sizes and charges of ions were introduced in order to obtain a dense structure, which may further change their NLO properties. Unexpectedly, compound 3 is constructed from the [Ga{B₅O₉(OH)}{BO(OH)₂}]^{2−} cluster and Na⁺ and Cs⁺

cations, and exhibits a rare 1D structure in GBOs with the CS space group. Attempts to produce compounds at higher temperatures using stronger bases or other alkali and alkaline earth metals were fruitless. It seems that the template effect is improved after adding the alkali or alkaline earth metal salt, which is not conducive to the formation of high-dimensional NCS borates under this condition.

Crystal structure of 1

Compound 1 is the precursor of 2. Single-crystal XRD analysis shows that 1 crystallizes in the centrosymmetric (CS) cubic space group *Pa*3̄. The asymmetric unit of compound 1 consists of two B atoms, 10/3 O atoms, 1/6 K⁺, 1/3 H₂O, and 1/2 H₃O⁺. BVS calculations show that K and B are consistent with the expected oxidation states.^{38,39} Three BO₄ units [B–O(av.), 1.471 Å] are joined together through corner-sharing of the μ₃-O4 atom and three BO₄ units are connected with neighboring three BO₃ units [B–O(av.), 1.366 Å] to form a compact cluster of [B₆O₁₃]^{8−} ({B₆}-1), with shorthand notation of 6:[3Δ + 3T)] (Fig. 1a). In {B₆}-1 clusters, the μ₃-O4–B bonds are unique because their bond distances (1.530 Å) are longer than those of the μ₂-O–B bonds (1.358–1.457 Å) in BO₃ and BO₄. Each {B₆}-1 is connected to six other {B₆}-1 by corner-sharing O3 atoms to form a 3D framework with misplaced 9-membered ring (9-MR) windows (Fig. 1b–d). The overall 3D framework can be rationalized as a *pcu* topology with the Schläfli symbol of (4¹²·6³) and the cubic cavity with a diameter of 8.60 Å is constructed from eight {B₆}-1 interconnected by O atoms (Fig. S1a and b†). The larger K⁺ ion in 1 (ionic radius: K⁺/1.38 Å, Na⁺/1.02 Å) makes the

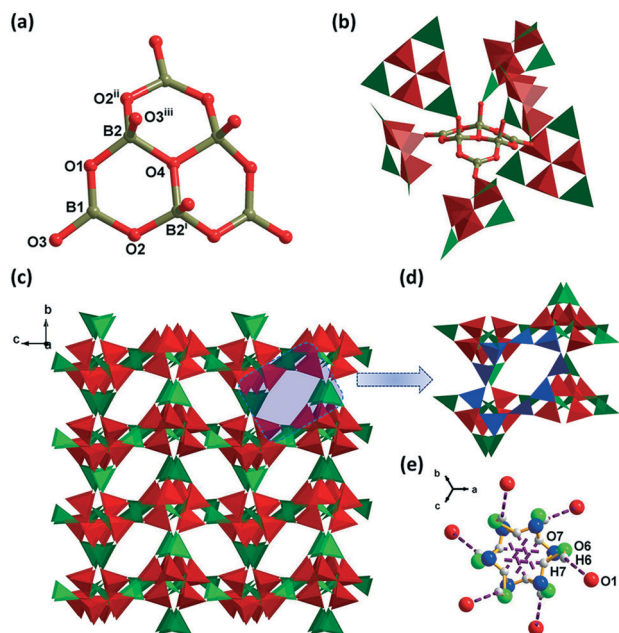


Fig. 1 (a) The structure of $\{B_6\}$ -1 of compound **1**, symmetry codes: (i) y, z, x ; (ii) z, x, y ; (iii) $y, -z + 1/2, x - 1/2$. (b) The linkage of $\{B_6\}$ -1. (c) The 3D framework viewed along the a axis. (d) The misplaced 9-MR windows highlighted with blue color. (e) The water cluster of **1**.

diameter of the cubic cavity longer (8.60 Å) than that in our previously reported $NH_4NaB_6O_{10}$ (7.35 Å).⁴⁰ Further, the structure is stabilized by the water cluster formed by $O6 \cdots H6$ (2.460 Å, 3.265 Å, 158°) and $O7-H7 \cdots O7$ (1.800 Å, 2.266 Å, 117°) hydrogen bonds among the water molecule, hydronium and $\{B_6\}$ -1 (Fig. 1e, Table S4†). The channels of **1** are also filled with guest ions/molecules of K^+ , water molecules and hydroniums (Fig. S1c†).

Crystal structure of 2

Considering that compound **1** crystallizes in the CS space group with a 3D framework, we tried to introduce a chiral GaO_4 polyhedron, and use its chiral induction and transfer characteristics to construct compounds crystallized in the NCS space group. As expected, one of the BO_4 groups of the $[B_6O_{13}]^{8-}$ cluster was substituted by GaO_4 , and then one BO_3 triangle is transplanted to link two BO_4 groups by corner-sharing, forming the acentric $[GaB_5O_{13}]^{8-}$ cluster in compound **2** (Fig. 2a and d). The new compound **2** crystallizes in the NCS monoclinic space group Pc and the $[GaB_5O_{13}]^{8-}$ cluster can be considered as the transfiguration of the centrosymmetric $[B_6O_{13}]^{8-}$ cluster. Each $[GaB_5O_{13}]^{8-}$ is connected to six others by corner-sharing O1, O6 and O7 atoms to form a 3D framework (Fig. 2b and f), and the 3D framework can also be regarded as having a pcu topology with the Schläfli symbol of $(4^{12} \cdot 6^3)$, just similar to **1**. As for the $[GaB_5O_{13}]^{8-}$ cluster, a GaO_4 polyhedron is particularly important for the structural expansion of compound **2**, which extends the 1D $[B_5O_{10}]^{5-}$ chain to a 3D framework by Ga–O–B bonds (Fig. 2c). In addition to the fact that **1** and **2** crystallize

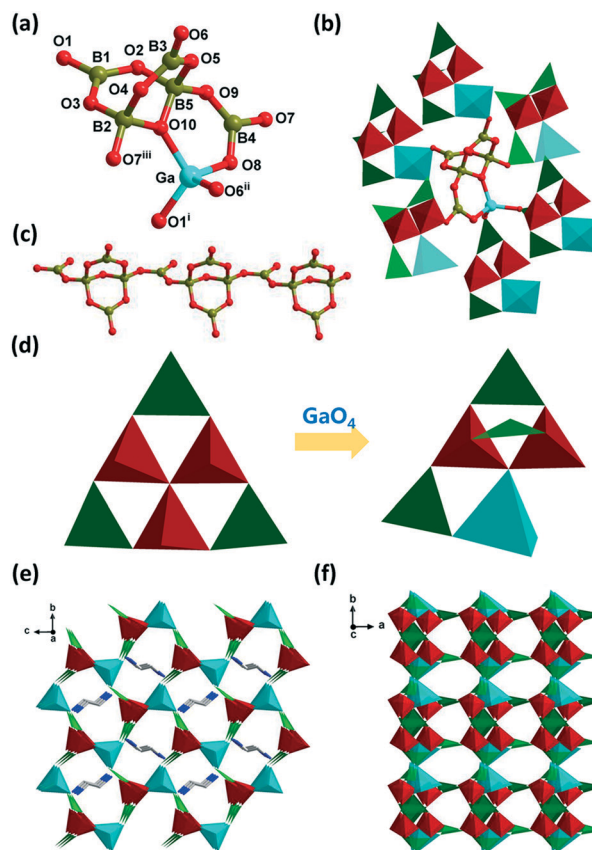


Fig. 2 (a) The structure of $[GaB_5O_{13}]^{8-}$ of compound **2**, symmetry codes: (i) $x, 1 - y, -0.5 + z$; (ii) $x, -y, -0.5 + z$; (iii) $1 + x, y, z$. (b) The linkage of the $[GaB_5O_{13}]^{8-}$ cluster. (c) The 1D chain formed by the oxoboron cluster. (d) Transformation from $[B_6O_{13}]^{8-}$ to $[GaB_5O_{13}]^{8-}$ by replacing a BO_4 with a GaO_4 group. (e) The 10-MR channels of the 3D framework located by the H_2en cations along the a axis. The H atoms are omitted for clarity. (f) View of the 9-MR channels along the c axis. Color code: BO_4 : red, BO_3 : green, GaO_4 : turquoise, similarly hereinafter.

in different space groups, their structures are also somewhat different. In **2**, a 3D-intersecting channel system contains a 10-, 9- and 9-MR along the a , b and c axes, respectively (Fig. 2e, f and S2†), and the template H_2en (en = ethylenediamine) cations interact with the 10-MR channels through several $N-H \cdots O$ (1.810–2.390 Å, 2.693–3.275 Å, 151–175°) hydrogen bonds (Table S5†). Meanwhile only the misplaced 9-MR windows can be observed in **1** along the a , b and c axes, and the shapes of the windows are also different (Fig. 1d). Besides, unlike compound **1**, there is no cavity structure in **2**. Therefore, the introduction of a chiral GaO_4 polyhedron changed the space group and the crystal structure of the compound.

Table 2 shows the structure of known ABOs and GBOs containing $[AlB_5O_{10}]$ and $[GaB_5O_{10}]$, respectively.^{8,41–45} Clearly, although the FBBs of the compound are $[MB_5O_{10}]$ ($M = Al, Ga$), they crystallize in a variety of space groups with different windows and different topological structures. The non-framework volumes and SHG responses are also different, which is related to the differences of templates and

Table 2 The structure of known $[\text{AlB}_5\text{O}_{10}]$ and $[\text{GaB}_5\text{O}_{10}]$

Formula	Space group	<i>n</i> -MR	Topology/net type	Non-framework volume (%)	SHG responses (\times KDP)	Ref.
$[\text{CH}_3\text{NH}_3]_{1.5}[\text{CH}_3\text{CH}_2\text{CH}_2\text{NH}_3]_{0.5}[\text{H}_2\text{O}]_5[\text{AlB}_5\text{O}_{10}]$	<i>P6</i> ₃	8, 9, 24	Zeolite CAN	63.4	1.1	41
$(\text{H}_3\text{APEA})_6[\text{AlB}_5\text{O}_{10}]_9 \cdot 12\text{H}_2\text{O}$	<i>P2</i> ₁	8, 11, 12	$\{4\cdot6^5\}_2\{6^6\}$	56.5	0.3	42
$(\text{HDETA})_2(\text{H}_2\text{DETA})_2[\text{AlB}_5\text{O}_{10}]_3$	<i>Pna2</i> ₁	11	<i>lon</i>	58.5	1.5	
$(\text{H}_2\text{EDAP})[\text{GaB}_5\text{O}_{10}] \cdot \text{H}_2\text{O}$ (2a)	<i>Pna2</i> ₁	8, 11	<i>dia</i>	51.4	0.5	
$\text{Al}[\text{B}_5\text{O}_{10}] \cdot \text{H}_2\text{dab} \cdot 2\text{H}_2\text{O}$	<i>P2</i> ₁ / <i>c</i>	8, 11, 12	<i>CrB</i> ₄	54.6 ^a	—	8
$[\text{Al}(\text{B}_4\text{O}_9)(\text{BO})] \cdot \text{H}_2\text{en}$ (2b)	<i>Pc</i>	9, 10	<i>pcu</i>	38.7 ^a	1.9	
$[\text{Al}(\text{B}_4\text{O}_9)(\text{BO})] \cdot \text{H}_2\text{dap}$	<i>Cc</i>	9, 10	<i>pcu</i>	44.9 ^a	2.1	
$\text{K}_2\text{Al}[\text{B}_5\text{O}_{10}] \cdot 4\text{H}_2\text{O}$	<i>C222</i> ₁	8, 11	<i>dia</i>	49.1 ^a	2.0	
$(\text{NH}_4)_2\text{Al}[\text{B}_5\text{O}_{10}] \cdot 4\text{H}_2\text{O}$	<i>C222</i> ₁	8, 11	<i>dia</i>	51.9 ^a	2.0	
$(\text{H}_2\text{TETA})[\text{AlB}_5\text{O}_{10}]$	<i>Pna2</i> ₁	8, 11, 14	<i>Sra</i>	57.2	1.5	43
$(\text{CH}_3\text{NH}_3)_2(\text{H}_2\text{O})_2[\text{AlB}_5\text{O}_{10}]$	<i>I4</i> ₂ <i>d</i>	8, 10	<i>dia</i>	52.6	2.0	44
$(\text{CH}_3\text{NH}_3)_2(\text{H}_2\text{O})[\text{AlB}_5\text{O}_{10}]$	<i>C2</i>	6, 8, 10, 11	<i>dia</i>	55.5	2.0	
$[\text{CH}_3\text{NH}_3][(\text{CH}_3\text{CH}_2)_2\text{NH}_2][\text{AlB}_5\text{O}_{10}]$	<i>Pbca</i>	8, 11, 14	<i>CrB</i> ₄	56.4	—	45
$[\text{CH}_3\text{CH}_2\text{NH}_3][(\text{CH}_3\text{CH}_2)_2\text{NH}_2][\text{AlB}_5\text{O}_{10}]$	<i>Pbca</i>	8, 11, 14	<i>CrB</i> ₄	56.4	—	
$[\text{CH}_3\text{CH}_2\text{NH}_3][(\text{CH}_3)_2\text{NH}_2](\text{H}_2\text{O})_{0.5}[\text{AlB}_5\text{O}_{10}]$	<i>Pbca</i>	8, 11, 14	<i>CrB</i> ₄	56.4	—	
$[\text{CH}_3\text{NH}_3][\text{CH}_3\text{CH}_2\text{NH}_3][\text{H}_2\text{O}]_2[\text{AlB}_5\text{O}_{10}]$	<i>Pna2</i> ₁	8, 14	<i>Sra</i>	54.7	0.5	
$[\text{GaB}_5\text{O}_{10}] \cdot \text{H}_2\text{en}$ (2)	<i>Pc</i>	9, 10	<i>pcu</i>	37.4	2.6	This work

^a Not mentioned in the references, but calculated in this work.

chiral polyhedra (AlO_4 , GaO_4) in compounds. Among them, compound **2** has the smallest non-framework volume and the highest SHG responses. Compared with our previous structure of $(\text{H}_2\text{EDAP})[\text{GaB}_5\text{O}_{10}] \cdot \text{H}_2\text{O}$ (**2a**, EDAP = *N*-ethyl-diaminopropane),⁴² they have some differences in structure and properties. Firstly, compound **2a** crystallizes in the orthorhombic *Pna2*₁ space group, while **2** crystallizes in the monoclinic *Pc* space group. Different space groups may lead to different asymmetric units and stacking structures. Secondly, for the B_5O_{10} cluster in **2a**, the central B atom adopts a tetrahedral geometry and is connected with two B_2O_5 groups, where the B atoms adopt a triangular geometry. The GaO_4 polyhedron further connects with one of the BO_3 of the B_5O_{10} cluster *via* the Ga–O–B bond (Fig. S3b†). Meanwhile in **2**, the B_4O_9 unit containing two BO_3 triangles (B1 and B3) and two BO_4 tetrahedra (B2 and B5) is linked by a BO_3 triangle (B4) *via* a μ_2 -O9 atom to form a $[\text{B}_4\text{O}_9(\text{BO}_2)]$ unit, this unit further chelates a chiral tetrahedral Ga center to form an acentric $[\text{GaB}_5\text{O}_{13}]^{8-}$ cluster through μ_2 -O8 and μ_3 -O10 atoms (Fig. S3a†). Thirdly, **2a** and **2** reveal two distinct shapes of the 8-MR and 9-MR channels because of different structure-directing agents (SDAs) (Fig. S3c and d†). As for the properties, due to different SDAs, en in **2** is significantly shorter than EDAP in **2a**, resulting in a smaller non-framework volume (**2**: 37.4%; **2a**: 51.4%) and a higher SHG response (**2**: $2.6 \times$ KDP; **2a**: $0.5 \times$ KDP). Compared with our other previous structure of $[\text{Al}(\text{B}_4\text{O}_9)(\text{BO})] \cdot \text{H}_2\text{en}$ (**2b**),⁸ the asymmetric unit and stacking structure of **2** and **2b** are similar. However, due to the different radii of the chiral center metal ions, the bond length of the Ga–O in **2** is longer than that of the Al–O bond in **2b** (**2**, Ga–O: 1.795–1.834 Å; **2b**, Al–O: 1.714–1.770 Å), and the pore dimension along the *a* axis in **2** is also larger than **2b** (**2**, 5.6×8.6 Å; **2b**, 2.3×5.6 Å). In addition, in terms of the NLO properties, the SHG response of **2** is also higher than **2b** (**2**: $2.6 \times$ KDP; **2b**: $1.9 \times$

KDP), indicating that the dense structure more easily forms materials with better NLO properties.

Crystal structure of **3**

Compound **3** is transformed from compound **2** by introducing Na^+ and Cs^+ . It crystallizes in the CS triclinic space group *P* $\bar{1}$. The asymmetric unit of **3** contains one $[\text{Ga}(\text{B}_5\text{O}_9(\text{OH}))\{\text{BO}(\text{OH})_2\}]^{2-}$, one Na^+ , and one Cs^+ , in which the $[\text{Ga}(\text{B}_5\text{O}_9(\text{OH}))\{\text{BO}(\text{OH})_2\}]^{2-}$ cluster is formed by $[\text{B}_5\text{O}_9(\text{OH})]^{4-}$ connected with $[\text{BO}(\text{OH})_2]^-$ through a GaO_4 tetrahedron (Fig. 3a). Each GaO_4 tetrahedron connects with three $[\text{B}_5\text{O}_9(\text{OH})]^{4-}$ and one $[\text{BO}(\text{OH})_2]^-$ (Fig. 3b). The $[\text{B}_5\text{O}_9(\text{OH})]^{4-}$, GaO_4 , and $[\text{BO}(\text{OH})_2]^-$ construct two opposite-orientated single chains with 8-MR channels along the *a* axis with dimensions of 3.5×8.2 Å through the linkage of $-\text{GaO}_4-\text{BO}_3-\text{BO}_4-\text{BO}_3-\text{GaO}_4-\text{BO}_3-\text{BO}_4-\text{BO}_3-$ (Fig. 3c and d). These two single chains can be considered as one inverted chain through an inversion center to obtain another chain. The double chains further extended to a 3D supramolecular framework by $\text{O1-H1}\cdots\text{O12}$ (1.974 Å, 2.766 Å, 163°), $\text{O13-H13}\cdots\text{O3}$ (1.945 Å, 2.761 Å, 176°), $\text{O12-H12}\cdots\text{O11}$ (2.408 Å, 2.974 Å, 127°), and $\text{O12-H12}\cdots\text{O9}$ (2.455 Å, 3.035 Å, 129°) hydrogen bonds with the distance between double chains of 8.0 Å (Fig. 3e and Table S6†).

In general, most ABOs/GBOs tend to form 2D or 3D structures *via* Al/Ga–O–B or Al–O–Al bonds (Table 3).^{31,32,42,46–49} So, a GBO with a 1D structure in **3** is rare. To the best of our knowledge, $[\text{Ga}(\text{en})_2][\text{B}_5\text{O}_8(\text{OH})_2] \cdot \text{H}_2\text{O}$ (**3a**) is the only GBO as well as ABO with a 1D structure so far.⁴⁹ The gallium(III) ion in **3a** is octahedrally coordinated with four N atoms from two en molecules and two O atoms from the $[\text{B}_5\text{O}_8(\text{OH})_2]^{3-}$ clusters (Fig. S4a†). The two chelated en molecules prevent the connection of the gallium(III) ion with other oxoboron clusters in the form of GaO_4 , thus

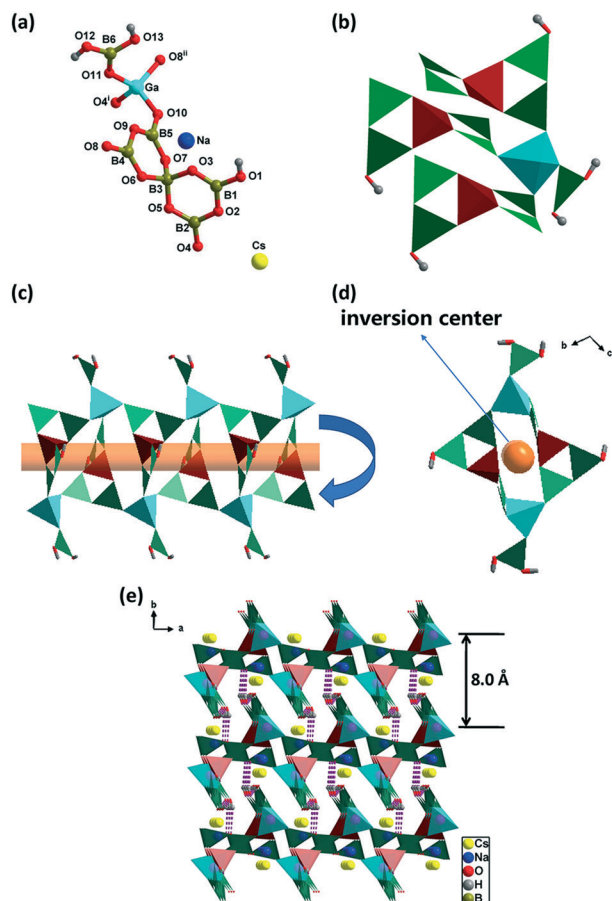


Fig. 3 (a) The asymmetric unit of **3**, symmetry codes: (i) $1 - x, 1 - y, 1 - z$; (ii) $1 + x, y, z$. (b) The linkage of GaO_4 . (c) 1D structure constructed from two opposite-orientated monolayers. (d) Inversion operation along the a axis with 8-MR channels. (e) The 3D supramolecular structure along the c axis connected by several $\text{O}-\text{H}\cdots\text{O}$ hydrogen bonds (dashed lines) with the charge balancing Na^+ and Cs^+ ions.

Table 3 The structure of known GBOs

Formula	Space group	GBO framework	Ref.
$[\text{Ga}_2\text{B}_7\text{O}_{14}(\text{OH})]\cdot\text{H}_2\text{1,6dah}$	$P\bar{1}$	2D	31
$\text{K}_2\text{Ga}_2\text{B}_7\text{O}_{14}(\text{OH})(\text{en})_{0.5}$	$P\bar{1}$	3D	
$(\text{H}_2\text{EDAP})[\text{GaB}_5\text{O}_{10}]\cdot\text{H}_2\text{O}$	$Pna2_1$	3D	42
$\text{Na}_4\text{Ga}_3\text{B}_4\text{O}_{12}(\text{OH})$	$F\bar{4}3c$	3D	46
$\text{BaGa}[\text{B}_4\text{O}_8(\text{OH})]\cdot\text{H}_2\text{O}$	$C2/c$	3D	32
$\text{BaGa}[\text{B}_4\text{O}_8(\text{OH})]\cdot(\text{H}_2\text{O})$	$P\bar{1}$	3D	47
$\text{Ba}_3\text{Ga}_2[\text{B}_3\text{O}_6(\text{OH})]_2[\text{B}_4\text{O}_7(\text{OH})_2]$	$Fdd2$	2D	48
$[\text{Ga}(\text{en})_2][\text{B}_5\text{O}_8(\text{OH})_2]\cdot\text{H}_2\text{O}$ (3a)	$P2_1/c$	1D	49
$\text{Rb}_2\text{Ga}(\text{B}_5\text{O}_{10})(\text{H}_2\text{O})_4$	$C222_1$	3D	
$\text{NaCs}[\text{Ga}\{\text{B}_5\text{O}_9(\text{OH})\}_2\{\text{BO}(\text{OH})_2\}]$ (3)	$P\bar{1}$	1D	This work

hindering the expansion of the structure of GBOs (Fig. S4b†). Further, two of the terminal oxygen atoms of $[\text{B}_5\text{O}_8(\text{OH})_2]^{3-}$ are protonated, that is another reason why **3a** cannot form a high-dimensional structure.

Compound **3** does not contain chelated organic amines, but has protonated oxoboron clusters and alkali metal

counterions, and also fails to form a high-dimensional structure. The possible reason for low-dimensional structure is that the synthesis temperature and alkalinity under this condition is not conducive to the dehydration and condensation of terminal hydroxyl groups of oxoboron clusters, so the alkali metal counterions are chosen to fill the chains of oxoboron clusters to balance the charge and block the expansion of the GBOs.

Compound characterization

The purity of compounds **1–3** are confirmed by powder XRD (Fig. S5†). The thermogravimetric (TG) curves and IR spectra of compounds **1–3** are discussed in the ESI† (Fig. S6 and S7). The UV/vis diffuse reflectance spectra of compounds **1–3** are shown in Fig. S8†. The band gaps obtained by extrapolating the linear part of the rising curve to zero for compounds **1–3** are 5.44, 4.91 and 5.14 eV, respectively, indicating that **1–3** are wide-band-gap semiconductors.^{8,31} Attempts to exchange the guest complexes of compound **2** with guest cations Li^+ / Na^+ / K^+ / Mg^{2+} / Ca^{2+} / Ba^{2+} were unsuccessful, mainly because the extensive H-bonds between the templates H_2en and the frameworks play an important role in stabilizing the structures.

Nonlinear optical properties

Compound **2** crystallizes in the NCS space group, the SHG measurement shows that **2** displays a SHG efficiency about 2.6 times that of KDP in the same particle range of 150–212 μm (Fig. 4). In order to understand the origin of the SHG efficiency after $\text{GaO}_4/\text{AlO}_4$ groups have been introduced into the oxoboron cluster backbone, the relationship between the macroscopic SHG behavior and acentric distortions of the building units is studied. According to the anionic-group theory,^{50–53} the BO_3 groups are responsible for the high SHG effect and the different orientation of the structure restricts their total NLO contribution. Therefore, we calculated the local dipole moments of BO_3 triangles, distorted GaO_4 and AlO_4 polyhedra in the unit

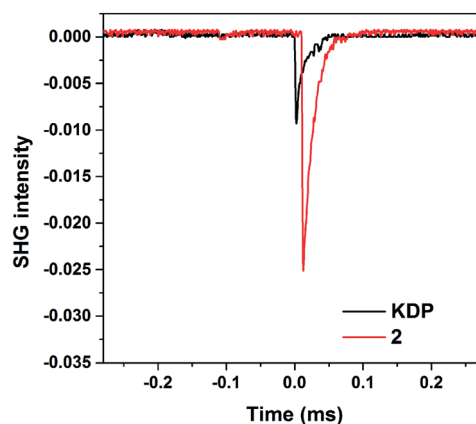


Fig. 4 Oscilloscope traces of SHG signals for compounds **2** and KDP in the same particle size range of 150–212 μm .

Table 4 The direction and magnitude (in Debye) of the polyhedral dipole moments for compounds **2** and **2b**

Species	<i>a</i>	<i>b</i>	<i>c</i>	Magnitude
Compound 2				
B1O ₃	-0.92×2	± 0.20	-0.83×2	1.26
B3O ₃	-0.02×2	± 0.45	-0.57×2	0.73
B4O ₃	0.49×2	± 0.28	-0.79×2	0.97
	-0.90	0	-4.38	
GaO ₄	-0.75×2	± 0.32	-0.58×2	1.00
	-1.50	0	-1.16	
Unit cell	-2.40	0	-5.54	6.04
Compound 2b				
B1O ₃	-0.52×2	± 0.21	-0.08×2	0.57
B3O ₃	-0.15×2	± 0.50	0.20×2	0.56
B5O ₃	0.54×2	± 0.26	-0.08×2	0.61
	-0.26	0	0.08	
AlO ₄	-1.13×2	± 0.15	-0.79×2	1.39
	-2.26	0	-1.58	
Unit cell	-2.52	0	-1.50	2.93

cells of **2** and **2b** based on the bond-valence approach (Table 4).^{38,39} Overall, the dipole moments of the building units are totally cancelled along the *b* axis in **2** and **2b**, while those are basically enhanced along the negative *a* and *c* axes. For **2b**, the calculated dipole moments for the BO₃ and AlO₄ groups are 0.56–0.61 D and 1.39 D (D = Debye), respectively. The AlO₄ groups are the main contribution of the SHG effect for **2b**. When a larger GaO₄ polyhedron is introduced into the crystal structure instead of smaller AlO₄, the calculated dipole moments for the BO₃ and GaO₄ groups are 0.73–1.26 D and 1.00 D in **2**, respectively. The component of the dipole moment of the unit cells on the negative *a* and *c* axes mainly comes from BO₃. Therefore, the larger total dipole moments of the unit cell make **2** (~2.6 times that of KDP, 6.04 D) show a relatively higher SHG response than **2b** (~1.9 times that of KDP, 2.93 D) as well as other ABOs containing the acentric [AlB₅O₁₃]⁸⁻ cluster (0.3–2.1 times that of KDP). The results show that an effective way to obtain a denser structure is by introducing larger metal ions into borates, and a dense structure more easily forms a desired NLO material with a higher SHG response in the presence of a chiral polyhedron.

Although KDP is widely used as the reference to estimate the SHG response, the disadvantage of KDP is its ability to adsorb water, which may have a certain effect on the study of NLO properties. Therefore, LiNbO₃ is more preferable as a sample for comparison than KDP. For the above reasons, we also characterized the SHG intensity of **2** at the commercial LiNbO₃ level. Compound **2** displays a SHG response about approximately 0.4 times that of commercial LiNbO₃ in the same particle range of 150–212 μm (Fig. S9†). Clearly, LiNbO₃ exhibits a significantly larger SHG response than KDP. As far as we know, it has been reported that most of the SHG responses of compounds are obtained at the KDP or LiNbO₃ level alone. The experimental results show that the SHG responses of LiNbO₃ is about 6.5 times that of KDP (2.6/0.4 = 6.5), which is basically consistent with a previous study (8.7 times).⁵⁴

Conclusions

In summary, two 3D framework borates K_{0.5}[B₆O₁₀]·H₂O·1.5H₂O (**1**) and [GaB₅O₁₀]·H₂en (**2**), and one 1D chain borate NaCs[Ga{B₅O₉(OH)}{BO(OH)₂}] (**3**) have been synthesized under mild solvothermal conditions. The structures of **2** and **3** were constructed on the basis of **1**. Compound **1** shows a 3D framework composed of [B₆O₁₃]⁸⁻ clusters, while one of the BO₄ groups of the [B₆O₁₃]⁸⁻ cluster was substituted by GaO₄, resulting in the acentric [GaB₅O₁₃]⁸⁻ cluster in **2**. The introduction of chiral GaO₄ polyhedra may induce and transfer the chirality to the oxoboron framework, which is beneficial to the formation of borates crystallized in the NCS space group. In addition, the 1D structure constructed from [Ga{B₅O₉(OH)}{BO(OH)₂}]²⁻ clusters in **3** is rare in GBOs as well as ABOs. What needs to be emphasized is that the calculations reveal that the dipole moments along the negative *a* and *c* axes are enhanced in **2**, which favor the relatively larger SHG response of **2** (~2.6 times that of KDP) than ABOs containing the acentric [AlB₅O₁₃]⁸⁻ cluster (0.3–2.1 times that of KDP). The larger atomic radius of **2** is more likely to form a dense structure, and thus the compound with better NLO properties can be obtained. We hope that this work is helpful to explore more new functional NLO materials with higher SHG responses.

Author contributions

Qi-Ming Qiu: Conceptualization, methodology, investigation, data curation, formal analysis, writing – original draft, preparation. Guo-Yu Yang: Writing – reviewing & editing, supervision, funding acquisition.

Conflicts of interest

There are no conflicts to declare.

Acknowledgements

This work was supported by the NSFC (No. 21571016, 21831001 and 91122028) and the NSFC for Distinguished Young Scholars (No. 20725101).

Notes and references

- J. Zhou, Y. Liu, H. Wu, H. Yu, Z. Lin, Z. Hu, J. Wang and Y. Wu, *Angew. Chem.*, 2020, **132**, 19168–19172.
- P. Ren, Y. Yang, M. Wen, H. Li, Z. Yang and S. Pan, *Inorg. Chem.*, 2020, **59**, 8396–8403.
- M. Gai, Y. Wang and S. Pan, *Chin. Sci. Bull.*, 2018, **63**, 998–1011.
- Y. Song, G. Yang, P. Gong, M. Luo, Z. Lin and N. Ye, *Inorg. Chem.*, 2020, **59**, 7789–7794.
- G. Zou and K. M. Ok, *Chem. Sci.*, 2020, **11**, 5404–5409.
- J. H. Huang, C. C. Jin, P. L. Xu, P. Gong, Z. Lin, J. W. Cheng and G. Y. Yang, *Inorg. Chem.*, 2019, **58**, 1755–1758.

- 7 B. B. Han, J. W. Cheng and G. Y. Yang, *CrystEngComm*, 2019, **21**, 1262–1266.
- 8 C. Rong, Z. Yu, Q. Wang, S. T. Zheng, C. Y. Pan, F. Deng and G. Y. Yang, *Inorg. Chem.*, 2009, **48**, 3650–3659.
- 9 Z. E. Lin, J. Zhang and G. Y. Yang, *Inorg. Chem.*, 2003, **42**, 1797–1799.
- 10 G. Zou and K. M. Ok, *Chem. Sci.*, 2020, **11**, 5404–5409.
- 11 H. Lee and K. M. Ok, *Bull. Korean Chem. Soc.*, 2020, **41**, 139–142.
- 12 Q. M. Qiu, X. Y. Li, C. A. Chen, K. N. Sun and G. Y. Yang, *J. Solid State Chem.*, 2021, **299**, 122193.
- 13 Q. M. Qiu and G. Y. Yang, *J. Solid State Chem.*, 2021, **301**, 122303.
- 14 Q. Wei, S. J. Sun, J. Zhang and G. Y. Yang, *Chem. – Eur. J.*, 2017, **23**, 7614–7620.
- 15 D. Qin, T. J. Zhang, C. B. Ma and G. Y. Yang, *Dalton Trans.*, 2020, **49**, 3824–3829.
- 16 C. A. Chen, R. Pan and G. Y. Yang, *Dalton Trans.*, 2020, **49**, 3750–3757.
- 17 H. A. Lehmann and A. Teske, *Z. Anorg. Allg. Chem.*, 1973, **400**, 169–175.
- 18 J. H. Wang, S. H. Feng and R. R. Xu, *J. Chem. Soc., Chem. Commun.*, 1989, 265–266.
- 19 J. H. Yu, R. R. Xu, Y. H. Xu and Y. Yue, *J. Solid State Chem.*, 1996, **122**, 200–205.
- 20 X. S. Liu and R. R. Xu, *J. Chem. Soc., Chem. Commun.*, 1989, 1837–1839.
- 21 J. H. Yu, R. R. Xu, Q. B. Kan and Y. Xu, *J. Mater. Chem.*, 1993, **3**, 77–82.
- 22 J. Ju, J. Lin, G. Li, T. Yang, H. Li, F. Liao, C. K. Loong and L. You, *Angew. Chem., Int. Ed.*, 2003, **42**, 5607–5610.
- 23 T. Yang, A. Bartoszewicz, J. Ju, J. Sun, Z. Liu, X. Zou, Y. Wang, G. Li, F. Liao, B. Martin-Matute and J. Lin, *Angew. Chem., Int. Ed.*, 2011, **50**, 12555–12558.
- 24 J. Ju, T. Yang, G. Li, F. Liao, Y. Wang, L. You and J. Lin, *Chem. – Eur. J.*, 2004, **10**, 3901–3906.
- 25 T. Yang, J. Ju, G. Li, F. Liao, X. Zou, F. Deng and J. Lin, *Inorg. Chem.*, 2007, **46**, 4772–4774.
- 26 W. Gao, Y. Wang, G. Li, F. Liao, L. You and J. Lin, *Inorg. Chem.*, 2008, **47**, 7080–7082.
- 27 J. Zhou, W. H. Fang, C. Rong and G. Y. Yang, *Chem. – Eur. J.*, 2010, **16**, 4852–4863.
- 28 L. Cheng and G. Y. Yang, *Chem. Commun.*, 2014, **50**, 344–346.
- 29 L. Wei, Q. Wei, Z. E. Lin, Q. Meng, H. He, B. F. Yang and G. Y. Yang, *Angew. Chem., Int. Ed.*, 2014, **53**, 7188–7191.
- 30 Y. Chen, Z. W. Guo, X. X. Li, S. T. Zheng and G. Y. Yang, *CCS Chem.*, 2021, **3**, 1232–1241.
- 31 C. A. Chen, R. Pan, T. J. Zhang, X. Y. Li and G. Y. Yang, *Inorg. Chem.*, 2020, **59**, 18366–18373.
- 32 Q. Wei, L. Li, L. Cheng, Q. Meng and G. Y. Yang, *Dalton Trans.*, 2014, **43**, 9427–9430.
- 33 W. Gao, Y. Jing, J. Yang, Z. Zhou, D. Yang, J. Sun, J. Lin, R. Cong and T. Yang, *Inorg. Chem.*, 2014, **53**, 2364–2366.
- 34 Q. Wei, J. W. Cheng, C. He and G. Y. Yang, *Inorg. Chem.*, 2014, **53**, 11757–11763.
- 35 H. Q. Wu, H. He, B. F. Yang and G. Y. Yang, *Inorg. Chem. Commun.*, 2013, **23**, 77–79.
- 36 G. M. Sheldrick, *Acta Crystallogr., Sect. C: Struct. Chem.*, 2015, **71**, 3–8.
- 37 A. L. Spek, *J. Appl. Crystallogr.*, 2003, **36**, 7–13.
- 38 I. D. Brown and D. Altermatt, *Acta Crystallogr., Sect. B: Struct. Sci.*, 1985, **41**, 244–247.
- 39 N. E. Brese and M. O'Keeffe, *Acta Crystallogr., Sect. B: Struct. Sci.*, 1991, **47**, 192–197.
- 40 J. H. Wang, J. W. Cheng, Q. Wei, H. He, B. F. Yang and G. Y. Yang, *Eur. J. Inorg. Chem.*, 2014, 4079–4083.
- 41 G. J. Cao, Q. Wei, J. W. Cheng, L. Cheng and G. Y. Yang, *Chem. Commun.*, 2016, **52**, 1729–1732.
- 42 L. Cheng and G. Y. Yang, *Inorg. Chem.*, 2018, **57**, 13505–13512.
- 43 Q. Meng, G. M. Wang, B. F. Yang, H. He and G. Y. Yang, *Inorg. Chem. Commun.*, 2014, **40**, 168–171.
- 44 G. J. Cao, J. Lin, J. Y. Wang, S. T. Zheng, W. H. Fang and G. Y. Yang, *Dalton Trans.*, 2010, **39**, 8631–8636.
- 45 G. J. Cao, J. Lin, W. H. Fang, S. T. Zheng and G. Y. Yang, *Dalton Trans.*, 2011, **40**, 2940–2946.
- 46 S. J. Yu, X. Y. Gu, T. T. Deng, J. H. Huang, J. W. Cheng and G. Y. Yang, *Inorg. Chem.*, 2017, **56**, 12695–12698.
- 47 T. T. Deng, Y. E. Gao, L. X. Zhang, X. Y. Gu, H. R. Tian, Y. Liu, Y. L. Feng and J. W. Cheng, *CrystEngComm*, 2014, **16**, 5689–5694.
- 48 L. Cheng, Q. Wei, H. Q. Wu, L. J. Zhou and G. Y. Yang, *Chem. – Eur. J.*, 2013, **19**, 17662–17667.
- 49 T. Hu, C. L. Hu, F. Kong, J. G. Mao and T. C. W. Mak, *Inorg. Chem.*, 2012, **51**, 8810–8817.
- 50 N. Ye, Q. X. Chen, B. C. Wu and C. T. Chen, *J. Appl. Phys.*, 1998, **84**, 555–558.
- 51 C. T. Chen, Y. C. Wu and R. K. Li, *Int. Rev. Phys. Chem.*, 1989, **5**, 65–91.
- 52 Y. Liu, Y. Shen, S. Zhao and J. Luo, *Coord. Chem. Rev.*, 2020, **407**, 213152.
- 53 L. Kang, F. Liang, X. Jiang, Z. Lin and C. Chen, *Acc. Chem. Res.*, 2020, **53**, 209–217.
- 54 W. J. Alford and A. V. Smith, *J. Opt. Soc. Am. B*, 2001, **18**, 524–533.